Dalton Transactions

Cite this: *Dalton Trans.*, 2012, **41**, 3562

www.rsc.org/dalton

PAPER

Tuning redox potentials of bis(imino)pyridine cobalt complexes: an experimental and theoretical study involving solvent and ligand effects†

C. Moyses Araujo,*[a] Mark D. Doherty,*[b] Steven J. Konezny,[a] Oana R. Luca,[a] Alex Usyatinsky,[b] Hans Grade,[b] Emil Lobkovsky,[c] Grigorii L. Soloveichik,*[b] Robert H. Crabtree[a] and Victor S. Batista*[a]

Received 16th November 2011, Accepted 14th January 2012
DOI: 10.1039/c2dt12195f

The structure and electrochemical properties of a series of bis(imino)pyridine Co^{II} complexes (NNN)CoX_2 and $[(NNN)_2Co][PF_6]_2$ (NNN = 2,6-bis[1-(4-R-phenylimino)ethyl]pyridine, with R = CN, CF_3, H, CH_3, OCH_3, $N(CH_3)_2$; NNN = 2,6-bis[1-(2,6-(*i*Pr)$_2$-phenylimino)ethyl]pyridine and X = Cl, Br) were studied using a combination of electrochemical and theoretical methods. Cyclic voltammetry measurements and DFT/B3LYP calculations suggest that in solution $(NNN)CoCl_2$ complexes exist in equilibrium with disproportionation products $[(NNN)_2Co]^{2+}$ $[CoCl_4]^{2-}$ with the position of the equilibrium heavily influenced by both the solvent polarity and the steric and electronic properties of the bis(imino)pyridine ligands. In strong polar solvents (*e.g.*, CH_3CN or H_2O) or with electron donating substituents (R = OCH_3 or $N(CH_3)_2$) the equilibrium is shifted and only oxidation of the charged products $[(NNN)_2Co]^{2+}$ and $[CoCl_4]^{2-}$ is observed. Conversely, in nonpolar organic solvents such as CH_2Cl_2 or with electron withdrawing substituents (R = CN or CF_3), disproportionation is suppressed and oxidation of the $(NNN)CoCl_2$ complexes leads to $18e^-$ Co^{III} complexes stabilized by coordination of a solvent moiety. In addition, the $[(NNN)_2Co][PF_6]_2$ complexes exhibit reversible $Co^{II/III}$ oxidation potentials that are strongly dependent on the electron withdrawing/donating nature of the *N*-aryl substituents, spanning nearly 750 mV in acetonitrile. The resulting insight on the regulation of redox properties of a series of bis(imino)pyridine cobalt(II) complexes should be particularly valuable to tune suitable conditions for reactivity.

Introduction

Understanding the redox properties of earth-abundant transition metal complexes is a challenge of great current interest, central to a wide range of applications in electrocatalysis.[1] An important goal is to establish fundamental principles to tune redox potentials and catalytic activity by modifying the ligands, or solvent conditions. In particular, there is a lot of current interest in the development of catalysts for direct organic proton exchange membrane (PEM) fuel cells where oxidation of an organic fuel provides the protons and electrons necessary to drive O_2 reduction to water.[2] However, the development of electrocatalysts capable of oxidizing organic fuels such as isopropanol or cyclohexane[2c,d] is hindered by a lack of understanding of the conditions that regulate the redox properties of earth-abundant transition metal complexes. This paper explores a series of Co complexes with bis(imino)pyridine ligands (Chart 1), with emphasis on the analysis of their electrochemical properties as influenced by the solvent, or ligand substituents with electron withdrawing/donating properties.

There is a sizable body of work documenting the utility of various transition metal complexes of bis(imino)pyridine ligands. Independently, Brookhart and Gibson have demonstrated that such complexes, particularly those containing *N*-aryl substituents with halides of iron(II) and cobalt(II), upon activation with methylaluminoxane (MAO) serve as precatalysts for α-olefin homopolymerization,[3] dimerization,[4] oligomerization[3c,4b,5] and co-polymerization with polar monomers.[3c,f] Derivatization of the *N*-aryl groups resulted in numerous substitution patterns[3g] and established the role that steric bulk at the *ortho* positions plays in determining catalyst activity, selectivity and, in the case of polymerization catalysts, polymer molecular weight.[3b,d,e,h,i] Further studies have focused on preparing reduced iron or cobalt alkyl complexes, particularly methyl

[a]*Department of Chemistry, Yale University, New Haven, CT 06520. E-mail: carlos.araujo@yale.edu, victor.batista@yale.edu*
[b]*General Electric Global Research, 1 Research Circle, Niskayuna, NY 12309. E-mail: doherty@ge.com, soloveichik@ge.com*
[c]*Department of Chemistry and Chemical Biology, Cornell University, Ithaca, NY 14853*

†Electronic supplementary information (ESI) available: The supporting information includes X-ray crystallographic files (CIF) for $[(\mathbf{1f})_2Co][CoCl_4]$ and **2g**, a table containing the electrochemical reduction potentials for compounds **2a–d**, **f**, **g** and **3a**, overlaid CV's of **2f** and **4f** in dichloromethane, ^1H NMR spectra of paramagnetic complexes, gas phase energies, Gibbs free energy upon solvation, and coordinates of the optimized computational structural models. CCDC 854625 (**2g**) and 854626 ($[(\mathbf{1f})_2Co][CoCl_4]$). For ESI and crystallographic data in CIF or other electronic format see DOI: 10.1039/c2dt12195f

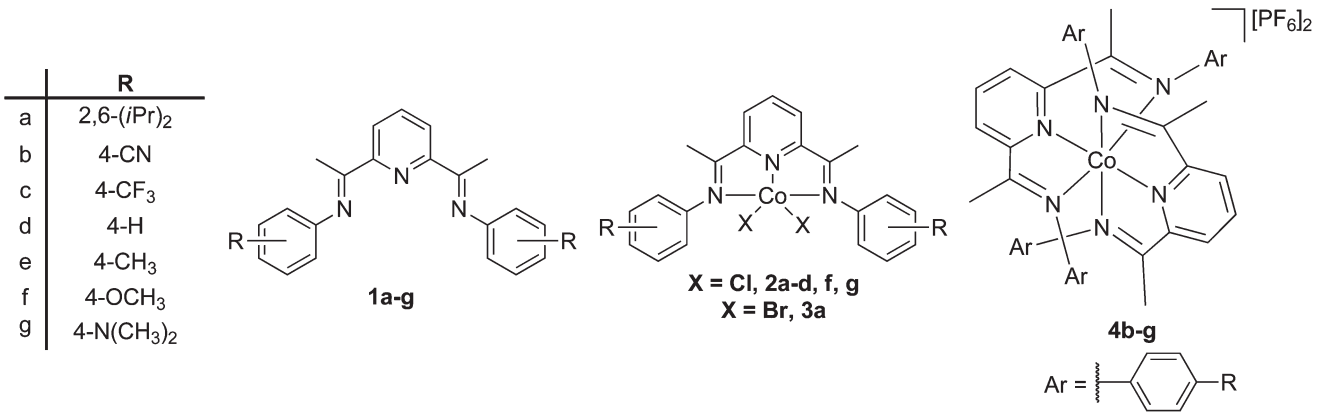

Chart 1 NNN ligands **1a–g**, (NNN)$Co^{II}X_2$ complexes **2a–d**, **f**, **g** and **3a**, and $[(NNN)_2Co^{II}][PF_6]_2$ complexes **4b–g** examined in this work.

complexes, as models of the propagating species present in the olefin polymerization systems described above.[6] Interest in these reduced compounds has grown to include detailed investigations into the electronic structure, redox properties and reactivity of the iron and cobalt complexes and has established the redox activity of these ligands.[6e,7]

More recently, several new applications of these bis(imino) pyridine transition metal complexes have been reported including a report by Chirik and co-workers in which they demonstrated C–H bond activation *via* thermolysis and photolysis of bis(imino) pyridine cobalt azide complexes.[8] In addition, highly efficient catalytic olefin hydrogenation has been achieved with bis(imino)pyridine iron bis(dinitrogen) complexes.[9] Related bis (imino)pyridine iron(II) triflate complexes have also shown some activity in the oxidation of cyclohexane with H_2O_2 to cyclohexanol and cyclohexanone, presumably through a Fenton type free radical mechanism.[10] Therefore, it is natural to expect that a wide range of applications could benefit from fundamental understanding of the dependence of the redox properties of these metal pincer complexes on the nature of the ligands, and on solvent conditions. While previous studies have analyzed the electronic structures associated with various possible oxidation states of cobalt bis(imino)pyridine complexes,[7c,e] a systematic study of the regulation of redox potentials as influenced by changes in the ligand framework or solvent environment is lacking.

In that context we report here an experimental and theoretical examination of the influence of electrostatic, steric and electronic factors on the redox potentials of a series of Co(NNN)X_2 and $[(NNN)_2Co][PF_6]_2$ (NNN is a tridentate bis(imino)pyridine ligand) complexes as shown in Chart 1. We examined ligands with different electron withdrawing or donating substituents and solvents of different polarity ranging from nonpolar to polar protic solvents (*e.g.* CH_2Cl_2, CH_3CN and H_2O). While many studies of these Co^{II} complexes have dealt with their reduction and subsequent chemical reactivity,[6b,7b,c,8] our interest lies in ultimately being able to oxidize liquid organic fuels for energy storage purposes.[2a] Therefore we have chosen to focus on the $Co^{II/III}$ redox couple and factors that contribute to one's ability to tune the oxidation potentials of these transition metal complexes.

Results and discussion

Synthesis and electrochemical characterization of (NNN)CoX_2 complexes

The (NNN)CoX_2 complexes were prepared in accordance with literature procedures for similar compounds by reaction of equal parts ligand and CoX_2 and the compounds examined in this study are shown in Chart 1 (see Experimental section for details). As expected, complexes **2a–d**, **f** and **g** are high spin and display paramagnetically broadened ^{1}H NMR spectra, with solution magnetic moments of 3.5–5.3 μ_B at 22 °C (Evans NMR method[11]), which is consistent with a high spin d^7 Co^{II} center.[3d,12]

One method of characterizing the redox activity of bis(imino) pyridine ligands is X-ray crystallography where reduced ligands exhibit bond distortions from neutral ligands. Black needle shaped single crystals suitable for single-crystal X-ray diffraction were obtained by vapor diffusion of diethyl ether into a saturated acetonitrile solution of **2g**. The molecular structure is shown in Fig. 1 while the collection and refinement parameters are collected in Table 6. Compound **2g** exhibits approximate C_s symmetry about the plane containing the cobalt, pyridyl nitrogen and two chlorine atoms. The geometry around the cobalt is best described as distorted trigonal bipyramidal with the equatorial plane formed by the pyridyl nitrogen and two chlorine atoms with $N_{pyridyl}$–Co–Cl angles of 130.79(5)° and 112.91(5)° and a Cl–Co–Cl angle of 116.23(3)°. Two axial Co–N_{imine} bonds fill out the cobalt(II) coordination sphere with an angle of 150.12 (7)°. A bond distance of 2.0344(18) Å for the Co–$N_{pyridyl}$ of **2g** is consistent with other *para* substituted complexes such as those reported for **2c**[13] and **2d**[14] and shorter than those reported for *ortho* substituted complexes such as **2a**.[3d] As with **2c**[13] and **2d**[14] the Co–N_{imine} bonds are slightly longer at 2.2093(18) and 2.2289(18) Å, while the C_{imine}–N_{imine} distances of 1.289(3) and 1.288(3) Å are typical for C=N double bonds of neutral bis (imino)pyridine ligands coordinated to first row transition metals.[7e] In addition, C_{imine}–C_{py} bond lengths of 1.488(3) and 1.489(3) Å and C_{py}–N_{py} bond lengths of 1.345(3) and 1.339(3) Å are consistent with the assignment of a neutral bis(imino)pyridine ligand.[7e] The *N*-aryl rings of **2g** exhibit dihedral angles of

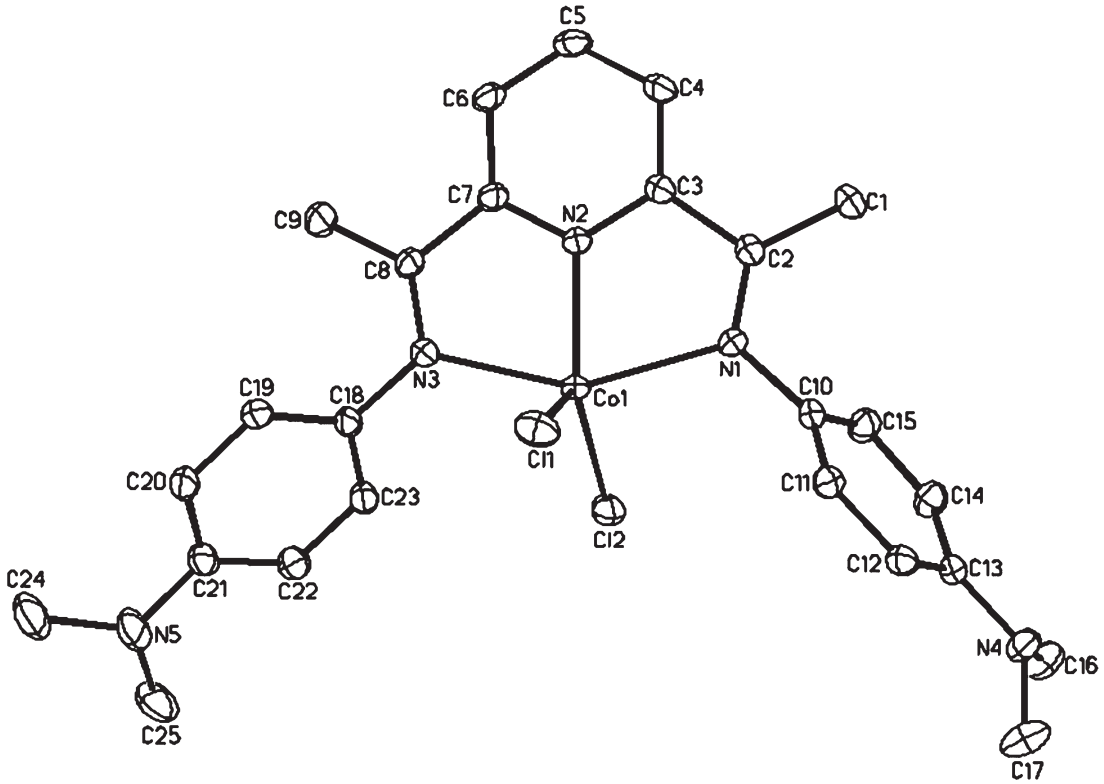

Fig. 1 ORTEP diagram of **2g** (40% probability ellipsoids). Hydrogen atoms have been removed for clarity. Selected bond distances (Å) and angles (°): Co(1)–N(1) 2.2093(18), Co(1)–N(2) 2.0344(18), Co(1)–N(3) 2.2289(18), Co(1)–Cl(1) 2.2733(6), Co(1)–Cl(2) 2.2562(6), N(1)–C(2) 1.289(3), C(2)–C(3) 1.488(3), C(3)–N(2) 1.345(3), N(2)–C(7) 1.339(3), C(7)–C(8) 1.489(3), N(3)–C(8) 1.288(2), N(2)–Co(1)–N(1) 75.03(7), N(2)–Co(1)–N(3) 75.55(3), (N1)–Co(1)–N(3) 150.11(7), N(2)–Co(1)–Cl(2) 130.79(5), N(1)–Co(1)–Cl(2) 94.46(5), N(3)–Co(1)–Cl(2) 100.75(5), N(2)–Co(1)–Cl(1) 112.91(5), N(1)–Co(1)–Cl(1) 99.53(5), N(3)–Co(1)–Cl(1) 96.58(5), Cl(2)–Co(1)–Cl(1) 116.23(3).

Table 1 Electrochemical data for **2a–d**, **f**, **g** and **3a** in acetonitrile and dichloromethane (0.1 M $[Bu_4N][BF_4]$ supporting electrolyte) *vs.* $Cp_2Fe^{0/+}$ at 0.1 V s^{-1} at a glassy carbon working electrode (d = 3 mm)

	CH_3CN		CH_2Cl_2		
	$Co^{II/III}$ (V)[a]	ΔE (mV)	$Co^{II/III}$ (V)[a]	ΔE (mV)	$\Delta Co^{II/III}$ (V)[b]
2a	+0.56	120	+0.70	152	+0.14
3a	+0.35[c]	N/A	+0.69[c]	N/A	+0.34
2b	+0.44[c]	N/A	+0.82[c]	N/A	+0.38
2c	+0.40[c]	N/A	+0.81[c]	N/A	+0.41
2d	+0.11	80	+0.67[c]	N/A	+0.56
2f	−0.01	70	−0.04	120	−0.03
2g	−0.19	60	−0.21	75	−0.02

[a] Half wave potentials, $E_{1/2}$, unless otherwise indicated. [b] $\Delta Co^{II/III} = Co^{II/III}{}_{DCM}–Co^{II/III}{}_{MeCN}$. [c] Irreversible oxidation, E_{PA}.

113.1 and 56.8° relative to the plane of the pyridine ring, which is consistent with those observed for other complexes lacking steric bulk at the *ortho* positions of the *N*-aryl ring **2d**.[14]

Cyclic voltammograms of 1 mM solutions of **2a–d**, **f** and **g** and **3a** exhibit $Co^{II/III}$ oxidation waves between −0.25 and +1.0 V *vs.* $Cp_2Fe^{0/+}$ in acetonitrile or dichloromethane (see Table 1). Replacing the chloride ligands with bromide ligands results in a Co^{II} center that is more easily oxidized (**2a** *vs.* **3a**), however, whereas **2a** exhibits a quasi-reversible oxidation wave in both solvents, oxidation of **3a** is electrochemically reversible in acetonitrile but irreversible in dichloromethane. Except for **2f** and **2g**, changing from acetonitrile to dichloromethane induces an anodic shift in the $Co^{II/III}$ oxidation potentials of +0.05 to +0.55 V, which we attribute to decreased stabilization of the developing cationic charge upon oxidation in a low polarity solvent such as dichloromethane. The slight cathodic shift of less than 50 mV observed for **2f** and **2g** upon moving to dichloromethane was unexpected and prompted a more detailed investigation.

Analysis of **2g** by matrix assisted laser desorption ionization time-of-flight (MALDI-TOF) mass spectrometry from an HBM–acetonitrile matrix (see Experimental section for details) revealed the presence of a species (*ca.* 15%) with m/z = 857 in addition to the expected m/z = 493 corresponding to $[\mathbf{2g} \neg Cl]^+$. This minor component, which does not contain any chlorine atoms, corresponds instead to $[(\mathbf{1g})_2Co]^+$. Similar analysis of **2f** showed the expected $[\mathbf{2f} \neg Cl]^+$ (m/z = 467) ions as well as the high m/z species with m/z = 805 corresponding to $[(\mathbf{1f})_2Co]^+$, which in this case is the major component at *ca.* 60%. Mass spectrometry analysis of **2d** showed only a minor amount of the high m/z species (<5% m/z = 685 $[(\mathbf{1d})_2Co]^+$, 95% m/z = 407 $[\mathbf{2d} \neg Cl]^+$) whereas **2c** and **2b** contained only the expected $[\mathbf{2c} \neg Cl]^+$ (m/z = 543) and $[\mathbf{2b} \neg Cl]^+$ (m/z = 457), respectively. As expected, complexes **2a** and **3a** exhibited only the anticipated $[\mathbf{2a} \neg Cl]^+$ (m/z = 575) and $[\mathbf{3a} \neg Cl]^+$ (m/z = 621) ions by mass spectrometry as a result of the steric bulk imparted by the *ortho* *i*-propyl groups that prohibit formation of any bis-ligand species.

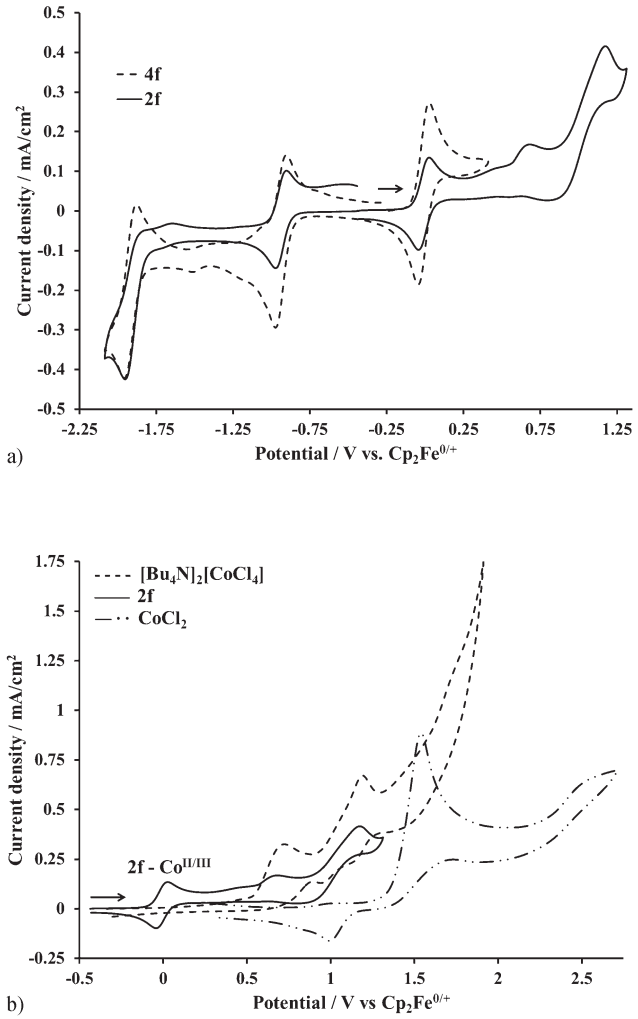

Fig. 2 Cyclic voltammograms of 1 mM solutions of (a) **2f** (—) and **4f** (- -) and (b) $[Bu_4N]_2[CoCl_4]$ (- -), **2f** (—) and $CoCl_2$ (— · ·) in acetonitrile with 0.1 M $[Bu_4N][BF_4]$ as supporting electrolyte and ν = 0.1 Vs^{-1} at a glassy carbon working electrode (d = 3 mm).

Close examination of the cyclic voltammogram (CV) of **2f** recorded in acetonitrile and comparison with literature data for **4f**[7e] and the CV of an authentic sample of **4f** (*vide infra*) shown in Fig. 2a indicates the presence of the $[(\mathbf{1f})_2Co]^{2+}$ dication in acetonitrile solutions of **2f**. In addition, anodic scans to higher potential reveal two electrochemically irreversible oxidations at +0.68 V and +1.17 V *vs.* $Cp_2Fe^{0/+}$. Given the reaction stoichiometry of 1 : 1 **1f** : $CoCl_2$, the presence of a $[(\mathbf{1f})_2Co]^{2+}$ dication suggests either outer sphere chloride anions and excess $CoCl_2$ or the formation of a tetrachlorocobaltate dianion, $[CoCl_4]^{2-}$ (eqn (1)). A cyclic voltammogram of $[Bu_4N]_2[CoCl_4]$ is shown in Fig. 2b overlaid with a CV of **2f** in acetonitrile, and shows two electrochemically irreversible oxidation waves at +0.72 V and +1.19 V *vs.* $Cp_2Fe^{0/+}$, which agrees with the assignment of a $[CoCl_4]^{2-}$ dianion. On the other hand, $CoCl_2$ (— · · in Fig. 2b) exhibits a sharp electrochemically irreversible oxidation at +1.54 V *vs.* $Cp_2Fe^{0/+}$ under similar conditions. Additional evidence for the formation of $[(\mathbf{1f})_2Co][CoCl_4]$ in acetonitrile solutions of **2f** can be gleaned from a comparison of the peak current densities for the $Co^{II/III}$ oxidation wave at +0.03 V. For a one electron transfer process with equimolar concentrations of **4f** and **2f**, the ratio of peak current densities, $i_{\mathbf{4f}}/i_{\mathbf{2f}} = 1$. Ligand redistribution of a 1 mM solution of **2f** to form 0.5 mM $[(\mathbf{1f})_2Co][CoCl_4]$ and comparison with a 1 mM solution of **4f** should give a ratio of peak current densities, $i_{\mathbf{4f}}/i_{\mathbf{2f}} = 2$. As illustrated in Fig. 2a, the ratio of peak current densities for 1 mM solutions of **4f** (i_{PA} = 0.273 mA cm^{-2}) and **2f** (i_{PA} = 0.135 mA cm^{-2}), $i_{\mathbf{4f}}/i_{\mathbf{2f}}$ is equal to 2 and is therefore most consistent with ligand disproportionation of **2f** to form $[(\mathbf{1f})_2Co][CoCl_4]$ in acetonitrile solution. A similar comparison of the CV of **2f** and **4f** in dichloromethane with 0.1 M $[Bu_4N][BF_4]$ as the supporting electrolyte indicates this ligand disproportionation reaction also occurs in dichloromethane (see Fig. S1 in ESI†).

$$2(NNN)CoCl_2 \rightleftharpoons [(NNN)_2Co][CoCl_4] \quad (1)$$

Attempts to obtain single crystals of **2f** by vapor diffusion of diethyl ether into a concentrated acetonitrile solution of **2f** resulted instead in red plate like crystals of the ion pair comprised of $[(\mathbf{1f})_2Co]^{2+}$ and $[CoCl_4]^{2-}$, the molecular structure of which is shown in Fig. 3 (see Table 6 for crystallographic data). Tetrahalometallate salts of $[(NNN)_2M]^{n+}$ have been observed previously for iron(II) complexes bearing NNN ligands that lack significant steric bulk in the 2,6 positions of the *N*-aryl rings (*e.g.* 2,2′;6′,2″-terpyridine[15] or 2,6-bis(2-(2-fluorophenylimino) ethyl)pyridine[16]). As expected the $[CoCl_4]^{2-}$ anion exhibits a slightly distorted tetrahedral geometry with nearly uniform Co–Cl bond lengths of 2.2759(10)–2.2867(10) Å and Cl–Co–Cl angles ranging from 105.74(4)° to 113.43(4)°. Although the $[(\mathbf{1f})_2Co]^{2+}$ cation has been structurally characterized previously as the hexafluorophosphate salt there are some significant differences in the metrical parameters of the cations in **4f**[7e] and $[(\mathbf{1f})_2Co][CoCl_4]$ reported here as shown in Table 2. Both structures display distorted octahedral geometries with two meridionally coordinated bis(imino)pyridine ligands with mutually *trans* pyridine nitrogens. The C_{py}–N_{py}, C_{imine}–C_{py} and C_{imine}–N_{imine} bond distances of the ligands in $[(\mathbf{1f})_2Co][CoCl_4]$ and **4f** do not show any substantial deviations from one another and are in agreement with the previous assignment of neutral bis(imino) pyridine ligands in the dication.[7e] However, the bis(imino)pyridine ligands are bound tighter in $[(\mathbf{1f})_2Co][CoCl_4]$ than in **4f**. One of the Co–N_{py} and three of the Co–N_{imine} distances are between 0.03 and 0.08 Å shorter in $[(\mathbf{1f})_2Co][CoCl_4]$ (1.913(2), 1.996(2), 1.989(2) and 2.135(2) Å) than in **4f** (1.991(2), 2.009 (2), 2.021(2) and 2.165(2) Å) while the remaining Co–N_{py} distance is equal.

Whereas the intraligand N_{py}–Co–N_{imine} and N_{imine}–Co–N_{imine} angles are in general only slightly larger (0.3 to 0.6°) in $[(\mathbf{1f})_2Co][CoCl_4]$ than in **4f**, important differences between the structures of these two cations are apparent upon comparison of the interligand N_{py}–Co–N_{py}, N_{py}–Co–N_{imine} and N_{imine}–Co–N_{imine} angles. The N_{py}–Co–N_{py} angle in $[(\mathbf{1f})_2Co][CoCl_4]$ (175.39(10)°) is farther from linearity than in **4f** (178.48(8)°). The average interligand N_{py}–Co–N_{imine} angles for **4f** and $[(\mathbf{1f})_2Co][CoCl_4]$ are 100.97(8)° and 100.73(10)°, respectively, however in **4f** each ligand is tilted slightly toward the Co–N_{py} bond of the other ligand and contains one large angle (N(2)–Co (1)–N(6) at 103.46(8)° and N(5)–Co(1)–N(3) at 100.91(8)°) and

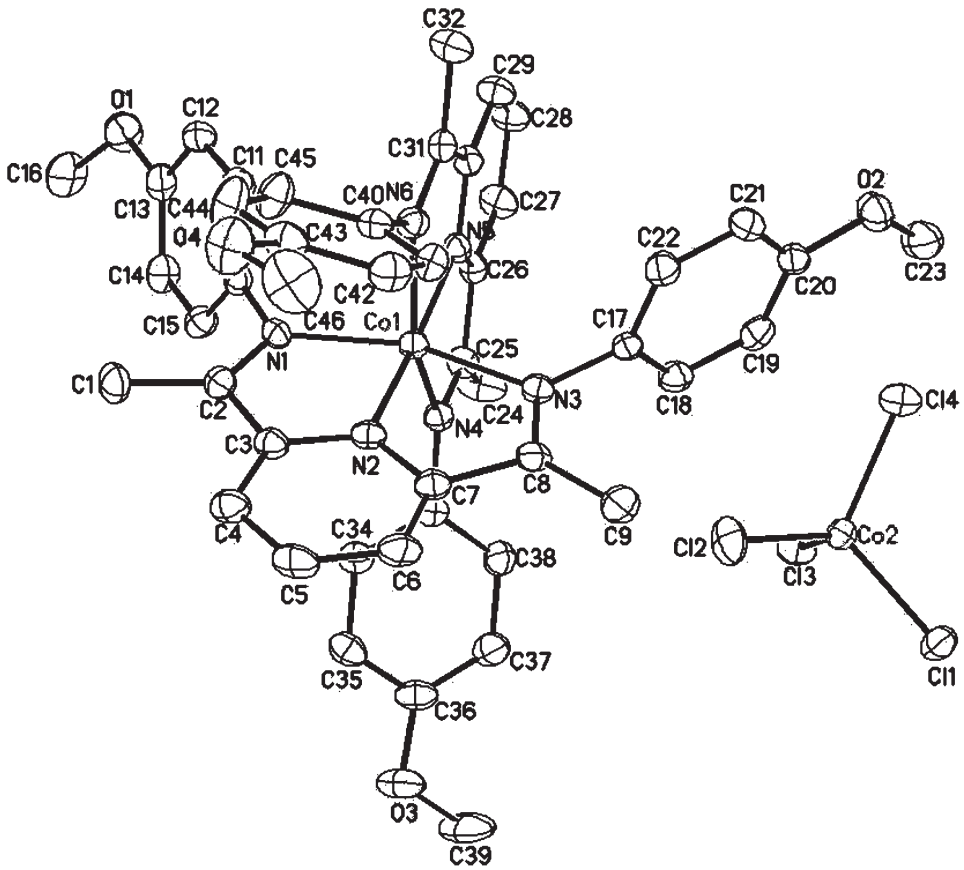

Fig. 3 ORTEP diagram of $[(\mathbf{1f})_2Co][CoCl_4]$ (40% probability ellipsoids). Hydrogen atoms and a molecule of acetonitrile have been removed for clarity. Metrical parameters for the cation are collected in Table 2 while selected bond distances (Å) and angles (°) for the anion follow: Co(2)–Cl(1) 2.2792(10), Co(2)–Cl(2) 2.2759(10), Co(2)–Cl(3) 2.2774(9), Co(2)–Cl(4) 2.2867(10), Cl(2)–Co(2)–Cl(3) 112.57(4), Cl(2)–Co(2)–Cl(1) 109.72(4), Cl(3)–Co(2)–Cl(1) 106.79(4), Cl(2)–Co(2)–Cl(4) 105.74(4), Cl(3)–Co(2)–Cl(4) 108.70(4), Cl(1)–Co(2)–Cl(4) 113.43(4).

one small angle (N(2)–Co(1)–N(4) at 100.97(8)° and N(5)–Co(1)–N(1) at 98.52(8)°). One ligand of $[(\mathbf{1f})_2Co][CoCl_4]$ is tilted more strongly toward the Co–N_{py} bond of the other ligand (N(2)–Co(1)–N(4) at 106.61(10)° and N(2)–Co(1)–N(6) at 97.20(10)°) while the imine nitrogens of the other ligand are virtually equidistant from N(5) (N(5)–Co(1)–N(1) at 99.92(10)° and N(5)–Co(1)–N(3) at 99.18(10)°). Finally, the N_{imine}–Co–N_{imine} angles show the most significant structural deviations between **4f** and $[(\mathbf{1f})_2Co][CoCl_4]$. As with the N_{py}–Co–N_{imine} angles, there are two large (N(1)–Co(1)–N(6) at 97.79(8)° and N(3)–Co(1)–N(4) at 97.11(8)°) and two small (N(1)–Co(1)–N(4) at 87.60(8)° and N(3)–Co(1)–N(6) at 85.73(8)°) N_{imine}–Co–N_{imine} angles in **4f**. These angles in $[(\mathbf{1f})_2Co][CoCl_4]$ differ from those in **4f** by 5.4° to 5.9° and are much closer to right angles (N(1)–Co(1)–N(4) at 93.47(9)°, N(1)–Co(1)–N(6) at 92.06(10)°, N(3)–Co(1)–N(4) at 91.21(9)° and N(3)–Co(1)–N(6) at 91.11(9)°) suggesting that the two bis(imino)pyridine ligands in $[(\mathbf{1f})_2Co][CoCl_4]$ are virtually orthogonal to one another and that the distortion from an ideal octahedral geometry is less pronounced than in **4f**.

Synthesis and electrochemical characterization of $[(NNN)_2Co][PF_6]_2$ complexes

In order to fully evaluate the contribution of the $[(NNN)_2Co]^{2+}$ ions to the electrochemical behavior of **2b–d**, **f** and **g**, the corresponding $[(NNN)_2Co][PF_6]_2$ complexes were prepared using the method reported by de Bruin[7e] for **4f** and are shown in Chart 1. The addition of two equivalents of ligand to $CoCl_2$ in methanol followed by excess ammonium hexafluorophosphate precipitates the product, which was collected by filtration, washed with cold methanol and air dried. As with **2a–d**, **f** and **g** these cobalt(II) complexes exhibit paramagnetically shifted ^1H NMR spectra, however the solution magnetic moments at 22 °C for **4b–g** are considerably smaller than those measured for the dichloride complexes and increase with decreasing electron donating ability from 2.1 μ_B for **4g** to 3.5 μ_B for **4b**. These data are consistent with a low spin d^7 Co^{II} center with $S = ½$ as previously observed for **4f**[7e] except for **4b**, which is better described as having a high spin $S = {}^3/_2$ ground state. This change in spin state is most likely the result of the strongly electron withdrawing 4-CN substituent in **4b** ($\sigma_p = 0.66$), which serves to stabilize the e_g (M–L σ*) orbitals and decrease the ligand field splitting. As will be discussed in more detail later, this also causes the half wave potential of **4b** to shift to more positive potentials relative to **4c–g** as it becomes more difficult to remove an electron from the stabilized σ* orbital.

As evidenced by the cyclic voltammograms shown in Fig. 4 and the data collected in Table 3, complexes **4b–g** exhibit much simpler redox chemistry. Each complex shows a reversible one-electron metal centered oxidation ($Co^{II/III}$) and one (**4c** and **e**) or

two (**4b**, **d**, **f** and **g**) reversible one-electron reductions. In accordance with previous electrochemical assignments for **4f**[7e], we assign the first reduction between −0.6 and −1.1 V *vs.* $Cp_2Fe^{0/+}$ as a metal centered reduction to $[Co^{I}(NNN^{0})_2]^{+}$, and the second reduction to a ligand centered process resulting in $[Co^{I}(NNN^{0})(NNN^{-1})]^{0}$. The $Co^{II/III}$ oxidation potential and first reduction potential (*e.g.* $[ML_2]^{+/2+}$) also show a strong correlation with the Hammett parameter[17] for the substituents in the *para* position of the *N*-aryl groups on the ligands as shown in Fig. 5. Replacing the *p*-H (σ_p = 0.00) on the *N*-aryl rings of **4d** with an electron withdrawing substituent induces an anodic shift of the $Co^{II/III}$ oxidation potential by as much as +0.28 V for **4b** with a *p*-CN (σ_p = 0.66). As highlighted previously, this is the result of stabilization afforded by the electron withdrawing substituents, which increases the potential required to remove an electron from the singly occupied e_g orbitals. Conversely, replacing the *p*-H with a donating substituent such as *p*-NMe_2 results in a cathodic shift of the $Co^{II/III}$ oxidation potential of approximately the same magnitude (−0.31 V, σ_p = −0.83) for **4g**. Here the destabilization provided by the electron donating substituents raises the energy of the singly occupied e_g orbitals allowing the oxidation to occur at much lower potentials.

Using the electrochemical data for **4b–g** as a point of reference it is now possible to reexamine the data in Table 1 for evidence of ligand redistribution to form $[(NNN)_2Co]^{2+}$ with **2b–d**, **f** and **g**. As with **2f** and in agreement with the mass spectrometry results (*vide supra*) the *N*,*N*-dimethylamino substituted **2g** also exhibits redox waves consistent with the formation of $[(\mathbf{1g})_2Co][CoCl_4]$ in acetonitrile (*cf.* Table 1: $Co^{II/III}$ = (−0.19 V and

Table 2 Selected bond distances (Å) and bond angles (°) for $[(\mathbf{1f})_2Co][CoCl_4]$ and **4f** and the minimum energy structure of **4f** obtained in the gas phase and at the B3LYP/lacvp-6-31g level of theory

	$[(\mathbf{1f})_2Co][CoCl_4]$	**4f**[7e]	**4f**(DFT)
	Bond distance		
	$Co–N_{py}$		
Co(1)–N(2)	1.852(2)	1.852(2)	1.899
Co(1)–N(5)	1.913(2)	1.991(2)	1.929
	$Co–N_{imine}$		
Co(1)–N(1)	1.996(2)	2.009(2)	2.146
Co(1)–N(3)	1.989(2)	2.021(2)	2.149
Co(1)–N(4)	2.191(2)	2.145(2)	2.236
Co(1)–N(6)	2.135(2)	2.165(2)	2.228
	$C_{imine}–N_{imine}$		
N(1)–C(2)	1.297(4)	1.298(3)	1.311
N(3)–C(8)	1.300(4)	1.305(3)	1.311
N(4)–C(25)	1.294(4)	1.289(3)	1.306
N(6)–N(31)	1.287(4)	1.289(3)	1.307
	$C_{imine}–C_{py}$		
C(2)–C(3)	1.469(4)	1.472(4)	1.476
C(7)–C(8)	1.476(4)	1.476(3)	1.477
C(25)–C(26)	1.487(4)	1.487(3)	1.482
C(30)–C(31)	1.487(4)	1.485(3)	1.481
	$C_{py}–N_{py}$		
N(2)–C(3)	1.349(4)	1.347(3)	1.356
N(2)–C(7)	1.347(4)	1.350(3)	1.358
N(5)–C(26)	1.348(4)	1.347(3)	1.359
N(5)–C(30)	1.346(4)	1.350(3)	1.359
	Bond Angle		
	$N_{py}–Co–N_{py}$ (*trans*)		
N(2)–Co(1)–N(5)	175.39(10)	178.48(8)	179.30
	$N_{imine}–Co–N_{imine}$ (*trans*)		
N(1)–Co(1)–N(3)	160.88(10)	160.56(8)	156.22
N(4)–Co(1)–N(6)	156.14(9)	155.54(8)	158.42
	$N_{py}–Co–N_{imine}$ (*cis*-intraligand)		
N(2)–Co(1)–N(1)	80.04(10)	80.42(8)	77.99
N(2)–Co(1)–N(3)	80.86(10)	80.42(8)	78.27
N(5)–Co(1)–N(4)	78.00(10)	77.45(8)	79.32
N(5)–Co(1)–N(6)	78.19(10)	78.16(8)	79.10
	$N_{py}–Co–N_{imine}$ (*cis*-interligand)		
N(2)–Co(1)–N(4)	106.61(10)	100.97(8)	101.36
N(2)–Co(1)–N(6)	97.20(10)	103.46(8)	100.20
N(5)–Co(1)–N(1)	99.92(10)	98.52(8)	102.05
N(5)–Co(1)–N(3)	99.18(10)	100.91(8)	101.68
	$N_{imine}–Co–N_{imine}$ (*cis*)		
N(1)–Co(1)–N(4)	93.47(9)	87.60(8)	88.42
N(1)–Co(1)–N(6)	92.06(10)	97.79(8)	96.02
N(3)–Co(1)–N(4)	91.21(9)	97.11(8)	94.73
N(3)–Co(1)–N(6)	91.11(9)	85.73(8)	89.10

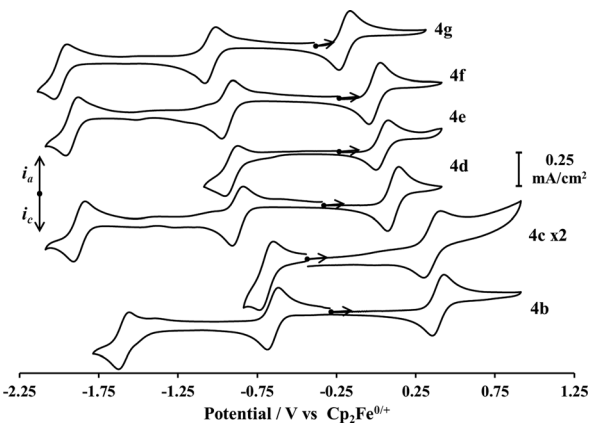

Fig. 4 Overlay of cyclic voltammograms of 1 mM solutions of **4b–g** recorded in acetonitrile with 0.1 M $[Bu_4N][BF_4]$ as supporting electrolyte and v = 0.1 Vs^{-1} at a glassy carbon working electrode (d = 3 mm).

Table 3 Electrochemical data for **4b–g** in acetonitrile (0.1 M $[Bu_4N][BF_4]$ supporting electrolyte) *vs.* $Cp_2Fe^{0/+}$ at 0.1 V s^{-1} at a glassy carbon working electrode (d = 3 mm)

	$[ML_2]^{0/+}$	ΔE (mV)	$[ML_2]^{+/2+}$	ΔE (mV)	$[ML_2]^{2+/3+}$	ΔE (mV)	σ_p[a]
4b	−1.59	70	−0.65	70	+0.39	75	0.66
4c	−1.69[c]	N/A	−0.70	90	+0.35	110	0.54
4d	−1.88	75	−0.87	70	+0.11	70	0.00
4e	−1.52[c]	N/A	−0.92	85	+0.03	80	−0.17
4f	−1.92	75	−0.94	70	−0.01	75	−-0.27
4g[b]	−1.99	80	−1.05	70	−0.20	75	−0.83

[a] See ref. 17. [b] This work and ref. 7e. [c] Irreversible reduction, E_{PC}.

Table S1†: E_{RED} = −1.13 V for **2g** and Table 3: $[ML_2]^{2+/3+}$ = −0.20 V and $[ML_2]^{+/2+}$ = −1.05 V for **4g** *vs.* $Cp_2Fe^{0/+}$) as well as dichloromethane (*cf.* Table 1: $Co^{II/III}$ = −0.21 V and Table S1†: E_{RED} = −1.02 V for **2g** *vs.* $Cp_2Fe^{0/+}$). In contrast, the CVs of **2b** and **2c** bearing strong electron withdrawing substituents do not exhibit any significant contributions from $[(\mathbf{1b})_2Co]^{2+}$ or $[(\mathbf{1c})_2Co]^{2+}$ in acetonitrile or dichloromethane, an observation that is also consistent with the mass spectrometry results. Interestingly, the CV of **2d**, which does not contain strongly donating or accepting substituents on the bis(imino)pyridine ligand, shows complete conversion to $[(\mathbf{1d})_2Co]^{2+}$ in acetonitrile (*cf.* Table 1: $Co^{II/III}$ = +0.11 V and Table S1†: E_{RED} = −0.88 V for **2d** and Table 3: $[ML_2]^{2+/3+}$ = +0.11 V and $[ML_2]^{+/2+}$ = −0.87 V for **4d** *vs.* $Cp_2Fe^{0/+}$) but not in dichloromethane (*cf.* Table 1: $Co^{II/III}$ = +0.67 V and Table S1†: E_{RED} = −0.08 V for **2d** *vs.* $Cp_2Fe^{0/+}$). While conversion of the (NNN)$CoCl_2$ complexes to the $[(NNN)_2Co][CoCl_4]$ salts appears to be more facile in acetonitrile than in dichloromethane, the electronic effects exerted by the bis(imino)pyridine substituents are also important and in the case of **2b** and **2c** the electronic effects are strong enough to prevent this ligand disproportionation.

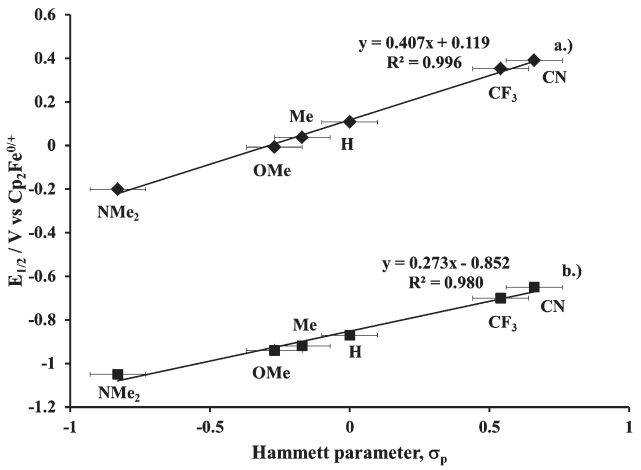

Fig. 5 Hammett plot correlating the (a) $[ML_2]^{2+/3+}$ (*e.g.* $Co^{II/III}$) and (b) $[ML_2]^{+/2+}$ $E_{1/2}$ with σ_p for the ligand *N*-aryl *para* substituents.

Theoretical evaluation of electrochemical properties of (NNN)CoX_2 complexes

We have carried out a thorough analysis of the ligand binding free energies and redox potentials at the DFT/B3LYP level (Fig. 6), using the computational methodology based on implicit solvation models (see Experimental section for details).[18] We investigated (NNN)$Co^{II}Cl_2$ and $[(NNN)Co^{III}Cl_2]^+$ complexes in three solvents of increasing polarity (CH_2Cl_2: ε = 8.9, CH_3CN: ε = 37.5 and H_2O: ε = 80.4) and considered various reaction pathways involving solvent–ligand exchange and disproportionation. The results reported in Fig. 6 correspond to **2d** as a representative example for **2a-d**, **f** and **g**. Table 4 compares the bond lengths and angles obtained for the calculated minimum energy structure of **2d** to the corresponding X-ray structure obtained by Gong *et. al.*[14] The bond lengths and angles involving the bis(imino)pyridine ligand and the cobalt center in the DFT optimized structure of **2d** agree very well with the reported structure[14] (largest difference of *ca.* 0.03 Å and 0.1°, respectively) and are consistent with a neutral bis(imino)pyridine ligand environment.[7e] Although the bond lengths and angles involving the chloride ligands show substantial deviations from the reported structure by *ca.* 0.09 Å and 5–20°, respectively, these are likely the result of crystal packing forces not accounted for in the calculated structure. In agreement with experimental data, **2d** was calculated to be a 17e⁻ high spin Co^{II} quartet ground state (d^7, $S = {}^3/_2$) with a trigonal bipyramidal geometry, while the singlet

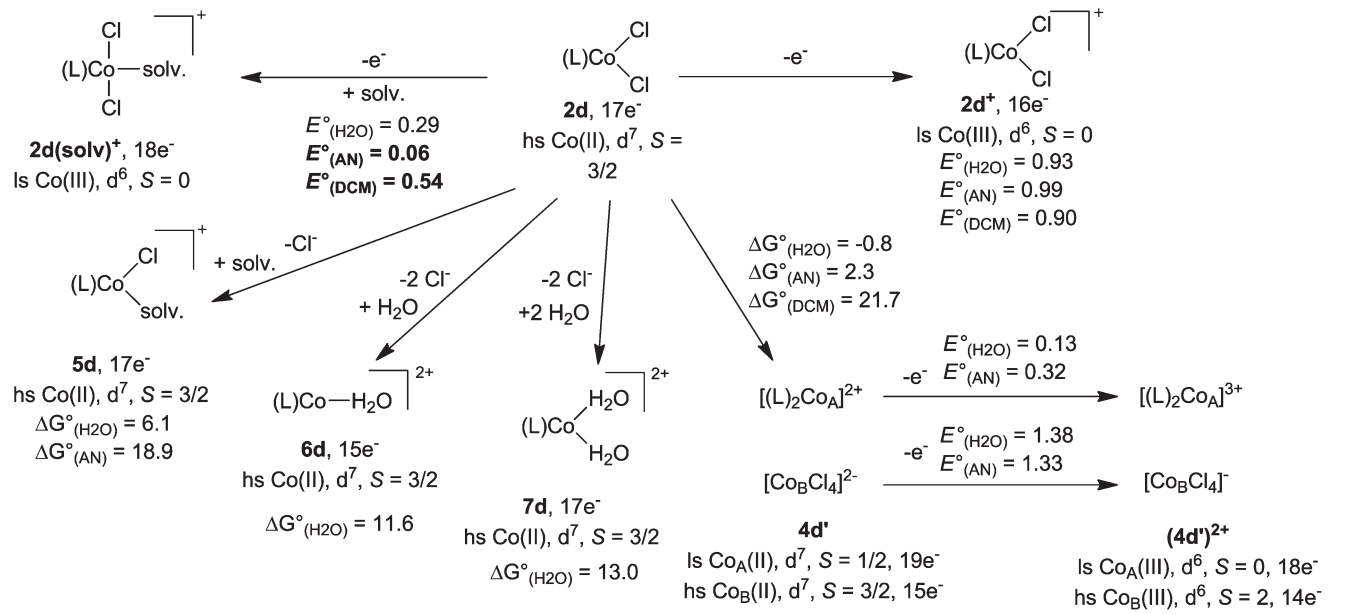

Fig. 6 The reaction pathways calculated for **2d** (L = **1d**) in CH_2Cl_2 (DCM), CH_3CN (AN), and H_2O, respectively. Free-energy changes ΔG are reported in kcal mol^{-1} and redox potentials, $E°$ in V *vs.* $Cp_2Fe^{0/+}$.

Table 4 Selected bond distances (Å) and bond angles (°) for **2d** and the minimum energy structure of **2d** obtained in the gas phase at the DFT B3LYP/lacvp-6-31G level of theory (elements labeled according to the reported structure)[14]

	2d[14]	**2d**(DFT)
Bond distance		
	$Co–N_{py}$	
Co(1)–N(2)	2.031(18)	2.050
	$Co–N_{imine}$	
Co(1)–N(1)	2.213(18)	2.241
Co(1)–N(3)	2.222(18)	2.242
	Co–Cl	
Co(1)–Cl(1)	2.268(6)	2.356
Co(1)–Cl(2)	2.261(6)	2.353
	$C_{imine}–N_{imine}$	
C(14)–N(2)	1.281(3)	1.299
C(6)–N(3)	1.281(3)	1.300
	$C_{imine}–C_{py}$	
C(1)–C(6)	1.494(3)	1.492
C(5)–C(14)	1.496(3)	1.487
	$C_{py}–N_{py}$	
C(1)–N(1)	1.347(3)	1.350
C(5)–N(1)	1.335(3)	1.348
Bond angle		
	$N_{imine}–Co–N_{imine}$	
N(1)–Co(1)–N(3)	150.88(7)	151.40
	$N_{py}–Co–N_{imine}$	
N(2)–Co(1)–N(1)	75.29(7)	75.22
N(2)–Co(1)–N(3)	75.64(7)	75.26
$N_{py}–Co–Cl$		
N(2)–Co(1)–Cl(1)	118.36(5)	108.35
N(2)–Co(1)–Cl(2)	123.78(5)	112.54
	$N_{imine}–Co–Cl$	
N(1)–Co(1)–Cl(1)	97.85(5)	94.83
N(1)–Co(1)–Cl(2)	95.86(5)	90.50
N(3)–Co(1)–Cl(1)	97.31(5)	95.92
N(3)–Co(1)–Cl(2)	98.80(5)	99.66
	Cl–Co–Cl	
Cl(1)–Co(1)–Cl(2)	117.84(3)	138.70

state containing a low spin 16e$^-$ Co^{III} ion (d^6, $S = 0$) was determined to be the ground state electronic configuration for **2d**$^+$.

Fig. 6 shows that the direct oxidation of **2d** without changing the coordination sphere at cobalt (Fig. 6, **2d** → **2d**$^+$) would require a significantly higher potential (+0.90, +0.99 and +0.93 V *vs.* $Cp_2Fe^{0/+}$ for CH_2Cl_2, CH_3CN and H_2O, respectively) than observed experimentally (+0.67, +0.11 and +0.02 V *vs.* $Cp_2Fe^{0/+}$ for CH_2Cl_2, CH_3CN and H_2O, respectively). This is likely because direct oxidation, without changing the coordination sphere of the metal center, produces a relatively unstable 16-electron complex. In contrast, coordination of a solvent molecule (*e.g.*, CH_3CN or CH_2Cl_2) upon oxidation of **2d** to form the 18e$^-$ low spin octahedral Co^{III}-species **2d(solv)**$^+$ at potentials of +0.06 V (CH_3CN) and +0.54 V (CH_2Cl_2) *vs.* $Cp_2Fe^{0/+}$ (bold in Fig. 6) is in good agreement with the experimental data reported in Table 1. In H_2O, however, the comparison is less favorable and suggests that neither of the two reaction pathways discussed so far are the predominant mechanisms for oxidation of **2d** in water.

To analyze alternative reaction pathways for oxidation in water, we have explored the feasibility of Cl^-/H_2O ligand exchange (Fig 6, **2d** → **5d**, **6d**, **7d**) as well as the possibility of disproportionation (Fig 6, **2d** → **4d**) where two neutral **2d** complexes react to form the ions $[(NNN)_2Co]^{2+}$ and $[CoCl_4]^{2-}$ that comprise **4d′**. To investigate these pathways, we have calculated the Gibbs free energies and the results are shown in Fig. 6. Replacement of one chloride ligand by a solvent moiety to form **5d** was found to be thermodynamically disfavored, demanding Gibbs free-energy changes of 6.1 and 18.9 kcal mol^{-1} for H_2O and CH_3CN, respectively. Similar 'uphill' free-energy changes are predicted for the substitution of both chloride ligands by a single solvent moiety in **6d**, or exchange of both chloride ligands by water in **7d**. These results suggest that none of the ligand-exchange reactions are thermodynamically favored, leaving disproportionation to **4d′** as the most likely reaction in water. It should also be mentioned that ion pairing was not considered for this calculation *i.e.* the free energy of the ions $[(L)_2Co_A]^{2+}$ and $[Co_BCl_4]^{2-}$ were evaluated separately.

Table 5 Calculated free energies, $\Delta G°$ in kcal mol^{-1} for disproportionation of **2b**, **d**, **f** to [(**1b**, **d**, **f**)$_2$Co][$CoCl_4$]

Solvent	**2f** (R = 4-OCH_3)	**2d** (R = 4-H)	**2b** (R = 4-CN)
H_2O	−3.7	−0.8	1.6
CH_3CN	−0.9	2.3	6.4
CH_2Cl_2	16.9	21.7	28.3

We have also investigated the effect of solvent polarity on the disproportionation reaction shown in Fig. 6 (**2d** → **4d′**) in an effort to further investigate such a reaction mechanism. The calculated free-energy changes are collected in Table 5 and indicate that such a disproportionation is spontaneous in water ΔG = −0.8 kcal mol^{-1} and very likely to be observed to some extent even in acetonitrile ΔG = 2.3 kcal mol^{-1} (K_{eq} = 0.13). However, in non-polar or weakly polar solvents (*e.g.*, CH_2Cl_2) the reaction is predicted to be non-spontaneous, with a significant free-energy penalty of 21.7 kcal mol^{-1}. Furthermore, the $Co^{II/III}$ oxidation potential calculated for $[(NNN)_2Co^{II}]^{2+}$ in **4d′** in water (+0.13 V *vs.* $Cp_2Fe^{0/+}$) is only *ca.* 0.1 V higher than that determined experimentally (+0.02 V *vs.* $Cp_2Fe^{0/+}$) suggesting that in water **2d** disproportionates prior to oxidation. In contrast, oxidation in CH_2Cl_2 must follow the pathway where the 18e$^-$ Co^{III} cation is stabilized by coordination of a CH_2Cl_2 moiety upon $Co^{II/III}$ oxidation (*i.e.* **2d** → **2d(solv)**$^+$). Finally, in polar organic solvents (*e.g.*, CH_3CN) although oxidation to the solvated Co^{III} species (**2d** → **2d(solv)**$^+$) is calculated to be thermodynamically more favored, both pathways are likely accessible at equilibrium. These results agree nicely with the experimental observation of disproportionation of **2d** to **4d′** in acetonitrile but not in dichloromethane (*vide supra*).

In addition to the analysis of the effect of solvent polarity on the underlying reaction mechanism, we have explored the effect of ligand substituents on the resulting free-energy profiles. As can be seen from the data in Table 5 a similar effect of solvent polarity on the disproportionation is observed for **2b** and **2f**, with the reaction in water being the most favorable, while disproportionation in dichloromethane is least favorable. The effect of ligand substituents on the reaction is also in very good agreement with experimental observations as the data in Table 5 indicates that disproportionation is favored for electron donating substituents and disfavored for electron withdrawing substituents relative to the unsubstituted complex **2d**. The electron donating

Table 6 Crystallographic data and structural refinement parameters for $[(\mathbf{1f})_2Co][CoCl_4]$ and **2g**

	$[(\mathbf{1f})_2Co][CoCl_4]$	**2g**
Formula	$C_{48}H_{49}Cl_4Co_2N_7O_4$	$C_{25}H_{29}Cl_2CoN_5$
Formula weight	1047.60	529.36
Crystal system	Monoclinic	Monoclinic
Space group	$P2_1/n$	$P2_1/n$
Cell dimensions		
a (Å)	17.8237(15)	12.3191(4)
b (Å)	15.3342(14)	15.1565(5)
c (Å)	19.2414(16)	14.1316(5)
α (°)	90	90
β (°)	113.367(3)	107.0280(10)
γ (°)	90	90
V (Å^3)	4827.6(7)	2522.90(15)
Z	4	4
D_{calc} (Mg m^{-3})	1.441	1.394
μ (Mo K$_\alpha$) (mm^{-1})	0.960	0.915
Crystal dimensions (mm^3)	0.30 × 0.30 × 0.03	0.50 × 0.20 × 0.05
T (K)	173(2)	173(2)
θ range (°)	1.76 to 27.10	1.93 to 28.28
No. of rflns	42 880	24 507
No. of indep reflns	10 559	6267
R_1 ($I > 2\sigma(I)$)	0.0480	0.0375
wR_2 (all data)	0.1372	0.1094
GOF	1.094	1.003
Largest diff. peak, hole (eÅ^{-3})	1.643, −0.836	1.252, −0.358

effect of the methoxy substituent is strong enough in **2f** to make disproportionation spontaneous in water and acetonitrile, while the electron withdrawing effect of the cyano group is strong enough to discourage disproportionation in dichloromethane and acetonitrile.

These results are therefore consistent with oxidation of the $(NNN)CoX_2$ complexes in water following disproportionation to $[(NNN)_2Co][CoCl_4]$. In contrast, 18e$^-$ solvated Co^{III} cations are formed upon oxidation of the $(NNN)CoX_2$ complexes in CH_2Cl_2 and coordination of a solvent moiety (*e.g.* formation of **2d(solv)**$^+$ in Fig. 6). Finally, in polar organic solvents (*e.g.*, CH_3CN) both pathways are accessible *via* the equilibrium shown in equation 1, although formation of the solvated Co^{III} species $[(NNN)CoX_2(solv)]^+$ is predicted to be thermodynamically more favored.

Conclusions

The electrochemical properties of a series of $(NNN)CoX_2$ and $[(NNN)_2Co][PF_6]_2$ complexes have been investigated for ligands with various electron donating/withdrawing substituents, in solvents of low (CH_2Cl_2), high (CH_3CN) and very high (H_2O) polarity. Experimental and theoretical results show clear evidence of the regulation of $Co^{II/III}$ oxidation potentials using ligand effects and/or solvent polarity, affecting not only the electronic properties but also the stability of the complexes. Introducing substituents in the *para* position of the *N*-aryl ring allows one to vary the $Co^{II/III}$ oxidation potential of the $[(NNN)_2Co][PF_6]_2$ complexes by up to 750 mV in acetonitrile.

Calculations show that oxidation of the $(NNN)CoX_2$ complexes in CH_2Cl_2 and CH_3CN leads to expansion of the coordination sphere of the metal to accommodate a solvent molecule. However, complexes lacking bulky substituents in the *ortho* positions of the *N*-aryl rings (**2b–d**, **f** and **g**) are in equilibrium with $[(NNN)_2Co][CoCl_4]$ resulting from disproportionation, with the equilibrium constant heavily influenced by solvent polarity and ligand electronic effects. In acetonitrile, complexes bearing electron donating or neutral substituents (**2d**, **2f** and **2g**) form the bis-ligand complexes almost exclusively, while those bearing electron withdrawing substituents (**2b** and **2c**) have equilibria predominantly displaced towards the $(NNN)CoCl_2$ species, with only minor amounts (~5%) of $[(NNN)_2Co][CoCl_4]$. In agreement with our DFT results, oxidation of the latter two complexes follows a different reaction pathway which likely involves coordination of a solvent molecule as in **2d(solv)**$^+$. These results are also in agreement with the CV data of **4b–g**, mass spectrometry data for **2b–d**, **f** and **g**, and the single-crystal X-ray structure of $[(\mathbf{2f})_2Co][CoCl_4]$ (obtained from crystallizing $[(\mathbf{1f})_2Co][CoCl_4]$ from CH_3CN/Et_2O). In dichloromethane, the disproportionation is observed only for **2f** and **2g** complexes with strong electron donating substituents, while **2b–d** do not show any evidence for disproportionation.

Therefore, we conclude that although increasing the solvent polarity can reduce the oxidation potential by as much as 600 mV (+0.67 V, +0.11 and +0.02 V *vs.* $CpFe^{0/+}$ for CH_2Cl_2, CH_3CN, H_2O) the stability of the complexes $(NNN)CoX_2$ is jeopardized by polar solvents such as H_2O or CH_3CN. This ultimately leads to disproportionation into coordinatively saturated $[(NNN)_2Co][CoCl_4]$ salts, which may not have the desired catalytic properties. A safer way of modulating the redox potentials is by moving to more electron-donating groups in the substituents of the pincer ligands (*e.g.*, R = NMe_2 as in **2g**), increasing the electron-density at the metal center, thus generating a more easily oxidized Co^{II} center, while electron-withdrawing groups (*e.g.*, R = CN as in **2b**) produce the opposite effect. A caveat to such a strategy, however, is that steric effects (or lack thereof) imparted by ligand substituents may affect any potential catalytic activity.

Experimental methods

General considerations

Acetonitrile and dichloromethane were dried by passage over activated molecular sieves and degassed prior to use. Bu_4NBF_4 was recrystallized three times from ethanol and dried under vacuum at 120 °C over P_2O_5 for 3 d. Elemental analyses were performed by Galbraith Laboratories, Inc., in Knoxville, TN. All ^1H and $^{13}C\{^1H\}$ NMR spectra were recorded on a Bruker 400 MHz Avance spectrometer and referenced to residual $CHCl_3$ (δ 7.27) or CHD_2CN (δ 1.94) for ^1H and $CDCl_3$ (δ 77.16) for $^{13}C\{^1H\}$. Spectra of the paramagnetic complexes can be found in the ESI.† Solution magnetic moments were determined by Evans NMR method[11] using the residual solvent signal as the reference and although these are generally the result of a single experiment, in several cases the values obtained were checked against multiple independent experiments and found to be in agreement (±0.1 μ_B). MALDI time-of-flight mass spectra were acquired with an Applied Biosystems Voyager-DE STR mass spectrometer utilizing a nitrogen laser (λ = 334 nm) to ionize a

dried residue consisting of the analyte mixed with the HBM–acetonitrile matrix (20 mg mL^{-1}) from a polished stainless steel plate (HBM = 4-hydroxybenzylidenemalononitrile). Electrochemical measurements were conducted on an IviumStat Electrochemical Interface & Impedance Analyzer from Ivium Technologies and were carried out under an inert Ar or N_2 atmosphere using 0.1 M tetrabutylammonium tetrafluoroborate as the supporting electrolyte in acetonitrile or dichloromethane. Cyclic voltammetry experiments were performed in a beaker type cell with a working volume of 5 mL using a standard three-electrode cell with a glassy carbon disk (d = 3 mm) working electrode, platinum wire counter electrode and a homemade reference electrode consisting of Ag wire immersed in a 10 mM $AgNO_3$/0.1 M Bu_4NBF_4 electrolyte in acetonitrile separated from the bulk solution by a "thirsty" Vycor™ frit.

Single crystals suitable for X-ray diffraction were transferred from a crystallization vessel into a drop of viscose organic oil, transferred to a nylon loop and mounted on a Bruker X8 APEX II diffractometer (Mo Kα radiation) and cooled to −100 °C. Data collection and reduction were done using Bruker APEX2 and SAINT + software packages and corrected for absorption using SADABS. Structures were solved by direct methods and refined on F^2 by full matrix least-squares techniques using SHELXTL software package. All non-hydrogen atoms were refined anisotropically. Hydrogen atoms were found in a difference Fourier map and refined isotropically (Table 6).

Theoretical methods

The computational methods implemented in this study have been described previously.[18] Here, we outline the methodology only briefly.

The standard reduction potentials are obtained, as follows:

$$E^{\circ} = -\frac{\Delta G_{(\mathrm{solv})}(\mathrm{Red})}{nF} \quad (2)$$

where F and n are the Faraday constant (23.06 kcal mol^{-1} V^{-1}) and the number of electrons involved in the redox reaction, respectively, by evaluating the reduction free energies ΔG(red) using the Born–Haber thermodynamic cycle (illustrated in Scheme 1), as follows:

$$\Delta G_{(\mathrm{solv})}(\mathrm{Red}) = \Delta G_{(\mathrm{g})}(\mathrm{Red}) + \Delta G_{(\mathrm{s})}(\mathrm{Red}) - \Delta G_{(\mathrm{s})}(\mathrm{Ox}) \quad (3)$$

with $\Delta G_{(\mathrm{g})}(\mathrm{Red}) = \Delta U_{(\mathrm{g})}(\mathrm{Red}) + \mathrm{PV} - T\Delta S_{(\mathrm{g})}(\mathrm{Red})$. The vibrational, rotational and translational contributions (statistical mechanics contributions) were included in the calculation of internal energy and entropy. The solvation free energies of the oxidized and reduced species, $\Delta G_{(\mathrm{s})}(\mathrm{Ox})$ and $\Delta G_{(\mathrm{s})}(\mathrm{Red})$, were calculated using the PBF method as described below, except for the Cl^- ion and the hydration of H_2O, for which we have used experimental results.[19]

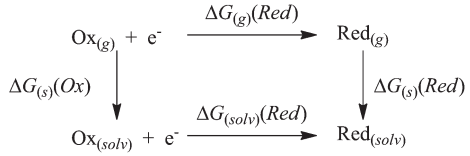

Scheme 1 Born–Haber thermodynamic cycle.

$$G = E_{\mathrm{elect}} + G_{\mathrm{solv}} + \mathrm{ZPVE} + \sum_{v} \frac{hv}{e^{hv/kT} - 1} + \frac{n}{2}kT - T(S_{\mathrm{vib}} + S_{\mathrm{rot}} + S_{\mathrm{trans}}) \quad (4)$$

where n = 8 accounts for the internal energies of the translational and rotational modes and the PV term. Calculated redox potentials are reported relative to $Cp_2Fe^{0/+}$, calculated at the same level of theory, to eliminate systematic differences due to the nature of the solvent, electrolyte and working electrode conditions.

All quantum chemistry calculations were carried out within the framework of density functional theory, using the hybrid density functional B3LYP[20] as implemented in the Jaguar 7.7 software package.[21] For geometry optimization and vibration calculations, we have employed a hybrid basis set where Co ions were described by LACVP effective core potential[22] and basis set (ECP), using the double-ζ contraction of valence functions, while the other elements (Cl, C, N and H) were treated in the level of 6-31G basis set.[23] Single-point calculations were also performed with a larger basis set cc-PVTZ(-f).[24]

Solvation energies were calculated using the Poisson–Boltzmann self-consistent reaction field method (PBF)[25] to represent the solvents with dielectric constant (effective radius) equal to 8.93 (2.33), 37.5 (2.19) and 80.37 (1.40) for dichloromethane (CH_2Cl_2), acetonitrile (CH_3CN) and water, respectively. Here, we have employed B3LYP/LACVP_cc-PVTZ(-f) theory level.

Synthetic procedures

Ligands **1a**,[3d,i] **1c**,[13] **1d**,[13,26] **1e**,[27] and **1f**[26] and complexes **2a**,[3d,i] **2c**,[13] **2d**,[13–14,26] **2f**,[26] **3a**[3b] and **4f**[7e] were prepared as reported previously while new ligands and complexes were prepared using modifications of these published procedures, the details of which are described below.

2,6-Bis[1-(4-cyanophenylimino)ethyl]pyridine, (1b)

2,6-Diacetylpyridine (2.00 g, 12.26 mmol, 1.0 equiv.), *p*-aminobenzonitrile (3.04 g, 25.75 mmol, 2.1 equiv.) and *p*-toluenesulfonic acid (0.010 g, 0.053 mmol, 0.05 equiv.) were dissolved in 70 mL of toluene and heated to reflux under N_2 with constant stirring and removal of water using a Dean–Stark trap. After 2 d, the reaction mixture was cooled to room temperature and the volatiles were removed by evaporation to give an orange-red residue. The addition of methanol and filtration of the resultant pale yellow solid, followed by washing with ethyl ether and petroleum ether gave 1.20 g (3.31 mmol, 27%) of a pale yellow powder. ^{1}H NMR ($CDCl_3$, 400.13 MHz, 24.4 °C) δ 8.36 (d, 2H, py-H_{meta}, $^3J_{HH}$ = 7.8 Hz), 7.93 (t, 1H, py-H_{para}, $^3J_{HH}$ = 7.8 Hz), 7.69 (d, 4H, *N*-Ar-H_{meta}, $^3J_{HH}$ = 8.5 Hz), 6.92 (d, 4H, *N*-Ar-H_{ortho}, $^3J_{HH}$ = 8.5 Hz), 2.41 (s, 6H, C(*Me*) = N). ^{13}C{^{1}H} NMR ($CDCl_3$, 100.6 MHz, 22.0 °C) δ 167.9, 155.3, 154.7, 137.2, 133.4, 123.1, 119.8, 119.2, 107.1, 16.6. MALDI MS, *m*/*z*: 364 [**1b** + H]$^+$.

2,6-Bis[1-(4-dimethylaminophenylimino)ethyl]pyridine, (1g)

2,6-Diacetylpyridine (2.00 g, 12.26 mmol, 1.0 equiv.), *N*,*N*-dimethyl-1,4-phenylene diamine (3.51 g, 25.75 mmol, 2.1 equiv.) and *p*-toluenesulfonic acid (0.010 g, 0.053 mmol, 0.05 equiv.) were dissolved in 70 mL of toluene and heated to reflux under N_2 with constant stirring and removal of water using a Dean–Stark trap. After 1 d, the reaction mixture was cooled to room temperature and the volatiles were removed by evaporation to give an orange-red residue. Addition of methanol and filtration of the resultant dark yellow solid, followed by washing with ethyl ether and petroleum ether gave 2.88 g (7.22 mmol, 59%) of a dark yellow powder. ^{1}H NMR ($CDCl_3$, 400.13 MHz, 24.4 °C) δ 8.32 (d, 2H, py-H_{meta}, $^3J_{HH}$ = 7.8 Hz), 7.84 (t, 1H, py-H_{para}, $^3J_{HH}$ = 7.8 Hz), 6.87 (d, 4H, *N*-Ar-H_{meta}, $^3J_{HH}$ = 9.1 Hz), 6.81 (d, 4H, *N*-Ar-H_{ortho}, $^3J_{HH}$ = 9.1 Hz), 2.98 (s, 12H, N(Me_2)), 2.49 (s, 6H, C(*Me*) = N). $^{13}C\{^1H\}$ NMR ($CDCl_3$, 100.6 MHz, 22.0 °C) δ 166.5, 156.0, 147.7, 141.0, 136.6, 121.8, 121.4, 113.2, 41.1, 16.3. MALDI MS, *m*/*z*: 400 [**1g** + H]$^+$.

2,6-Bis[1-(4-cyanophenylimino)ethyl]pyridine cobalt(II) chloride, (2b)

1b (0.75 g, 2.07 mmol, 1.001 equiv.) and $CoCl_2$ (0.27 g, 2.06 mmol, 1.0 equiv.) were combined in 65 mL of THF and stirred under N_2 overnight at room temperature. The reaction mixture was then poured into 125 mL of ethyl ether and the resulting precipitate was isolated by vacuum filtration, washed with ethyl ether and petroleum ether and air dried to give 1.02 g (2.06 mmol, 99%) of a green powder. Elemental analysis calcd for $C_{23}H_{17}Cl_2CoN_5$: C, 56.00; H, 3.47; N, 14.20. Found: C, 55.19; H, 3.49; N, 13.66.[28] MALDI MS, *m*/*z*: 457 [**2b** – Cl]$^+$. Magnetic susceptibility (acetonitrile-d_3, 297 K): μ_{eff} = 5.1 μ_B.

2,6-Bis[1-(4-dimethylaminophenylimino)ethyl]pyridine cobalt(II) chloride, (2g)

1g (1.00 g, 2.50 mmol, 1.0 equiv.) and $CoCl_2$ (0.33 g, 2.50 mmol, 1.0 equiv.) were combined in 70 mL of THF and stirred under N_2 overnight at room temperature. The reaction mixture was then poured into 150 mL of ethyl ether and the resulting precipitate was isolated by vacuum filtration, washed with ethyl ether and petroleum ether and air dried to give 1.18 g (2.23 mmol, 89%) of a brown powder. Elemental analysis calcd for $C_{25}H_{29}Cl_2CoN_5$: C, 56.72; H, 5.52; N, 13.23. Found: C, 57.00; H, 5.63; N, 13.01. MALDI MS, *m*/*z*: 493 [**2g** – Cl]$^+$, 857 [(**1g**)$_2$Co]$^+$. Magnetic susceptibility (acetonitrile-d_3, 297 K): μ_{eff} = 3.5 μ_B.

Bis{2,6-Bis[1-(4-cyanophenylimino)ethyl]pyridine}cobalt(II) hexafluorophosphate, 4b

1b (0.26 g, 0.71 mmol, 2.01 equiv.) and $CoCl_2$ (0.046 g, 0.35 mmol, 1.00 equiv.) were dissolved in 20 mL of methanol and the mixture was stirred at room temperature for 30 minutes before excess NH_4PF_6 (0.78 g, 4.82 mmol, 13.6 equiv.) was added to precipitate the product. The brick-red solid was collected by filtration, washed with ice cold methanol and air dried to give 0.382 g (0.35 mmol, 100%) of **4b**. Elemental analysis calcd for $C_{46}H_{34}CoF_{12}N_{10}P_2$: C, 51.36; H, 3.19; N, 13.02. Found: C, 50.90; H, 3.34; N, 12.55.[28] MALDI MS, *m*/*z*: 785 [**4b** – 2 PF_6]$^+$. Magnetic susceptibility (acetonitrile-d_3, 297 K): μ_{eff} = 3.5 μ_B.

Bis{2,6-Bis[1-(4-trifluoromethylphenylimino)ethyl]pyridine} cobalt(II) hexafluorophosphate, 4c

2c (0.30 g, 0.67 mmol, 2.04 equiv.) and $CoCl_2$ (0.042 g, 0.33 mmol, 1.00 equiv.) were dissolved in 25 mL of methanol and the mixture was stirred at room temperature for 30 minutes before excess NH_4PF_6 (0.81 g, 4.99 mmol, 15.3 equiv.) was added. The solution was dried under reduced pressure and the resulting red residue was taken up in dichloromethane, washed with water and the organic phase was dried with Na_2SO_4 and filtered. The filtrate was dried under reduced pressure and 0.38 g (0.30 mmol, 92%) of a red powder was obtained after trituration from a 1 : 1 diethyl ether : hexane mixture. Elemental analysis calc. for $C_{46}H_{34}CoF_{24}N_6P_2$: C, 44.28; H, 2.75; N, 6.74. Found: C, 44.13; H, 2.84; N, 6.39. MALDI MS, *m*/*z*: 957 [**4c** – 2 PF_6]$^+$, 1104 [**4c** – PF_6]$^+$. Magnetic susceptibility (acetonitrile-d_3, 297 K): μ_{eff} = 2.7 μ_B.

Bis{2,6-Bis[1-(phenylimino)ethyl]pyridine}cobalt(II) hexafluorophosphate, 4d

1d (0.14 g, 0.45 mmol, 2.3 equiv.) and $CoCl_2$ (0.025 g, 0.19 mmol, 1.00 equiv.) were dissolved in 20 mL of methanol and the mixture was stirred at room temperature for 30 minutes before excess NH_4PF_6 (0.52 g, 3.17 mmol, 16.5 equiv.) was added to precipitate the product. The brown crystalline solid was collected by filtration, washed with ice cold methanol and air dried to give 0.143 g (0.15 mmol, 76%) of **4d**. Elemental analysis calcd for $C_{42}H_{38}CoF_{12}N_6P_2$: C, 51.70; H, 3.93; N, 8.61. Found: C, 51.99; H, 3.98; N, 8.66. MALDI MS, *m*/*z*: 685 [**4d** – 2 PF_6]$^+$. Magnetic susceptibility (acetonitrile-d_3, 297 K): μ_{eff} = 2.6 μ_B.

Bis{2,6-Bis[1-(4-methylphenylimino)ethyl]pyridine}cobalt(II) hexafluorophosphate, 4e

1e (0.30 g, 0.88 mmol, 2.24 equiv.) and $CoCl_2$ (0.051 g, 0.39 mmol, 1.00 equiv.) were dissolved in 20 mL of methanol and the mixture was stirred at room temperature for 30 minutes before excess NH_4PF_6 (1.00 g, 6.17 mmol, 15.7 equiv.) was added to precipitate the product. The brick-red solid was collected by filtration, washed with ice cold methanol and air dried to give 0.258 g (0.25 mmol, 64%) of **4e**. Elemental analysis calcd for $C_{46}H_{46}CoF_{12}N_6P_2$: C, 53.55; H, 4.49; N, 8.15. Found: C, 53.04; H, 4.50; N, 8.02. MALDI MS, *m*/*z*: 741 [**4e** – 2 PF_6]$^+$. Magnetic susceptibility (acetonitrile-d_3, 297 K): μ_{eff} = 2.7 μ_B.

Bis{2,6-Bis[1-(4-dimethylaminophenylimino)ethyl]pyridine} cobalt(II) hexafluorophosphate, 4g

1g (0.39 g, 0.98 mmol, 2.02 equiv.) and $CoCl_2$ (0.063 g, 0.48 mmol, 1.00 equiv.) were dissolved in 20 mL of methanol

and the mixture was stirred at room temperature for 30 minutes before excess NH_4PF_6 (1.14 g, 7.03 mmol, 14.5 equiv.) was added to precipitate the product. The brick-red solid was collected by filtration, washed with ice cold methanol and air dried to give 0.346 g (0.30 mmol, 62%) of **4g**. Elemental analysis calcd for $C_{50}H_{58}CoF_{12}N_{10}P_2$: C, 52.31; H, 5.09; N, 12.20. Found: C, 51.31; H, 5.14; N, 11.98.[28] MALDI MS, *m/z*: 857 [**4g** ¬ 2 PF_6]$^+$, 1002 [**4g** ¬ PF_6]. Magnetic susceptibility (acetonitrile-d_3, 297 K): $\mu_{eff} = 2.1(4)\ \mu_B$.

Acknowledgements

This material is based upon work supported as part of the Center for Electrocatalysis, Transport Phenomena, and Materials (CETM) for Innovative Energy Storage, an Energy Frontier Research Center funded by the U.S. Department of Energy, Office of Science, Office of Basic Energy Sciences under Award Number DE-SC00001055.

References

1 G. Jerkiewicz, *Electrocatalysis*, 2010, **1**, 1.
2 (*a*) R. H. Crabtree, *Energy Environ. Sci.*, 2008, **1**, 134–138; (*b*) G. L. Soloveichik, J. P. Lemmon, J. -C. Zhao (General Electric Company), *USA Pat.*, 2008/0248339, 2008; (*c*) N. Kariya, A. Fukuoka and M. Ichikawa, *Chem. Commun.*, 2003, 690–691; (*d*) N. Kariya, A. Fukuoka and M. Ichikawa, *Phys. Chem. Chem. Phys.*, 2006, **8**, 1724–1730; (*e*) D. L. DuBois and R. M. Bullock, *Eur. J. Inorg. Chem.*, 2011, 1017–1027; (*f*) A. D. Wilson, R. H. Newell, M. J. McNevin, J. T. Muckerman, M. R. DuBois and D. L. duBois, *J. Am. Chem. Soc.*, 2006, **128**, 358–366; (*g*) B. R. Galan, J. Schoffel, J. C. Linehan, C. Seu, A. M. Appel, J. A. S. Roberts, M. L. Helm, U. J. Kilgore, J. Y. Yang, D. L. DuBois and C. P. Kubiak, *J. Am. Chem. Soc.*, 2011, **133**, 12767–12779.
3 (*a*) C. C. H. Atienza, C. Milsmann, E. Lobkovsky and P. J. Chirik, *Angew. Chem., Int. Ed.*, 2011, **50**, 8143–8147; (*b*) A. M. A. Bennett (DuPont), *WO Pat.*, 98/27124, 1998; (*c*) C. Bianchini, G. Giambastiani, I. G. Rios, G. Mantovani, A. Meli and A. M. Segarra, *Coord. Chem. Rev.*, 2006, **250**, 1391–1418; (*d*) G. J. P. Britovsek, M. Bruce, V. C. Gibson, B. S. Kimberley, P. J. Maddox, S. Mastroianni, S. J. McTavish, C. Redshaw, G. A. Sloan, S. Stromberg, A. J. P. White and D. J. Williams, *J. Am. Chem. Soc.*, 1999, **121**, 8728–8740; (*e*) G. J. P. Britovsek, V. C. Gibson, B. S. Kimberley, P. J. Maddox, S. J. McTavish, G. A. Solan, A. J. P. White and D. J. Williams, *Chem. Commun.*, 1998, 849–850; (*f*) G. J. P. Britovsek, V. C. Gibson, S. K. Spitzmesser, K. P. Tellmann, A. J. P. White and D. J. Williams, *J. Chem. Soc., Dalton Trans.*, 2002, 1159–1171; (*g*) V. C. Gibson, C. Redshaw and G. A. Solan, *Chem. Rev.*, 2007, **107**, 1745–1776; (*h*) B. L. Small and M. Brookhart, *Macromolecules*, 1999, **32**, 2120–2130; (*i*) B. L. Small, M. Brookhart and A. M. A. Bennett, *J. Am. Chem. Soc.*, 1998, **120**, 4049–4050.
4 (*a*) B. L. Small, *Organometallics*, 2003, **22**, 3178–3183; (*b*) K. P. Tellmann, V. C. Gibson, A. J. P. White and D. J. Williams, *Organometallics*, 2005, **24**, 280–286.
5 (*a*) B. L. Small and M. Brookhart, *J. Am. Chem. Soc.*, 1998, **120**, 7143–7144; (*b*) B. L. Small, R. Rios, E. R. Fernandez and M. J. Carney, *Organometallics*, 2007, **26**, 1744–1749.
6 (*a*) M. W. Bouwkamp, S. C. Bart, E. J. Hawrelak, R. J. Trovitch, E. Lobkovsky and P. J. Chirik, *Chem. Commun.*, 2005, 3406–3408; (*b*) M. J. Humphries, K. P. Tellmann, V. C. Gibson, A. J. P. White and D. J. Williams, *Organometallics*, 2005, **24**, 2039–2050; (*c*) T. M. Kooistra, Q. Knijnenburg, J. M. M. Smits, A. D. Horton, P. M. Budzelaar and A. W. Gal, *Angew. Chem., Int. Ed.*, 2001, **40**, 4719–4722; (*d*) J. Scott, S. Gambarotta, I. Korobkov and P. M. Budzelaar, *Organometallics*, 2005, **24**, 6298; (*e*) A. M. Tondreau, C. Milsmann, A. D. Patrick, H. M. Hoyt, E. Lobkovsky, K. Wieghardt and P. J. Chirik, *J. Am. Chem. Soc.*, 2011, **132**, 15046–15059.
7 (*a*) S. C. Bart, K. Chlopek, E. Bill, M. W. Bouwkamp, E. Lobkovsky, F. Neese, K. Wieghardt and P. J. Chirik, *J. Am. Chem. Soc.*, 2006, **128**, 13901–13912; (*b*) A. C. Bowman, C. Milsmann, C. C. H. Atienza, E. Lobkovsky, K. Wieghardt and P. J. Chirik, *J. Am. Chem. Soc.*, 2010, **132**, 1676–1684; (*c*) A. C. Bowman, C. Milsmann, E. Bill, E. Lobkovsky, T. Weyhermuller, K. Wieghardt and P. J. Chirik, *Inorg. Chem.*, 2010, **49**, 6110–6123; (*d*) P. M. Budzelaar, B. de Bruin, A. W. Gal, K. Wieghardt and J. L. van Lenthe, *Inorg. Chem.*, 2001, **40**, 4649–4655; (*e*) B. de Bruin, E. Bill, E. Bothe, T. Weyhermuller and K. Wieghardt, *Inorg. Chem.*, 2000, **39**, 2936–2947.
8 C. C. H. Atienza, A. C. Bowman, E. Lobkovsky and P. J. Chirik, *J. Am. Chem. Soc.*, 2010, **132**, 16343–16345.
9 (*a*) H. Nakazawa and M. Itazaki, in *Topics in Organometallic Chemistry: Iron Catalysis Fundamentals and Applications*, ed. B. Plietker, Springer, New York, NY, Editon edn, 2011, vol. 33, pp. 27–81; (*b*) R. J. Trovitch, E. Lobkovsky, E. Bill and P. J. Chirik, *Organometallics*, 2008, **27**, 1470–1478; (*c*) R. J. Trovitch, E. Lobkovsky and P. J. Chirik, *J. Am. Chem. Soc.*, 2008, **130**, 11631–11640; (*d*) S. C. Bart, E. Lobkovsky and P. J. Chirik, *J. Am. Chem. Soc.*, 2004, **126**, 13794–13807.
10 G. J. P. Britovsek, J. England, S. K. Spitzmesser, A. J. P. White and D. J. Williams, *J. Chem. Soc., Dalton Trans.*, 2005, 945–955.
11 (*a*) D. F. Evans, *J. Chem. Soc.*, 1959, 2003–2005; (*b*) S. K. Sur, *J. Magn. Reson.*, 1989, **82**, 169–173.
12 R. S. Drago, *Physical Methods for Chemists*, Surfside Scientific Publishers, Gainesville, FL, 2nd edn, 1992.
13 D. Gong, B. Wang, H. Cai, X. Zhang and L. Jiang, *J. Organomet. Chem.*, 2011, **696**, 1584–1590.
14 D. Gong, B. Wang, C. Bai, J. Bi, F. Wang, W. Dong, X. Zhang and L. Jiang, *Polymer*, 2009, **50**, 6259–6264.
15 W. M. Reiff, N. E. Erickson and W. A. Baker Jr, *Inorg. Chem.*, 1969, **8**, 2019–2021.
16 Y. Chen, R. Chen, C. Qian, X. Dong and J. Sun, *Organometallics*, 2003, **22**, 4312–4321.
17 (*a*) D. H. McDaniel and H. C. Brown, *J. Org. Chem.*, 1958, **23**, 420–427; (*b*) W. G. Herkstroeter, *J. Am. Chem. Soc.*, 1973, **95**, 8686–8691.
18 (*a*) T. Wang, G. Brudvig and V. S. Batista, *J. Chem. Theory Comput.*, 2010, **6**, 755–760; (*b*) T. Wang, G. Brudvig and V. S. Batista, *J. Chem. Theory Comput.*, 2010, **6**, 2395–2401.
19 (*a*) C. P. Kelly, C. J. Cramer and D. G. Truhlar, *J. Phys. Chem. B*, 2007, **111**, 408–422; (*b*) J. Sefcik and W. A. Goddard III, *Geochim. Cosmochim. Acta*, 2001, **65**, 4435–4443.
20 (*a*) A. D. Becke, *Phys. Rev. A: At., Mol., Opt. Phys.*, 1988, **38**, 3098–3100; (*b*) C. Lee, W. Yang and R. G. Parr, *Phys. Rev. B*, 1988, **37**, 785–789; (*c*) A. D. Becke, *J. Chem. Phys.*, 1993, **98**, 5648–5652.
21 Jaguar, Schrodinger, LLC, New York, NY, Editon edn., 2010.
22 P. J. Hay and W. R. Wadt, *J. Chem. Phys.*, 1985, **82**, 299–310.
23 (*a*) W. J. Hehre, R. Ditchfield and J. A. Pople, *J. Chem. Phys.*, 1972, **56**, 2257–2261; (*b*) M. M. Francl, W. J. Pietro, W. J. Hehre, J. S. Binkley, M. S. Gordon, D. J. DeFrees and J. A. Pople, *J. Chem. Phys.*, 1982, **77**, 3654–3665.
24 (*a*) T. H. Dunning Jr, *J. Chem. Phys.*, 1989, **90**, 1007–1023; (*b*) R. A. Kendall, T. H. Dunning Jr and R. J. Harrison, *J. Chem. Phys.*, 1992, **96**, 6796–6806; (*c*) D. E. Woon and T. H. Dunning Jr, *J. Chem. Phys.*, 1994, **100**, 2975–2988.
25 (*a*) D. J. Tannor, B. Marten, R. Murphy, R. A. Friesner, D. Sitkoff, A. Nicholls, M. Ringnalda, W. A. Goddard III and B. Honig, *J. Am. Chem. Soc.*, 1994, **116**, 11875–11882; (*b*) B. Marten, K. Kim, C. Cortis, R. A. Friesner, R. B. Murphy, M. N. Ringnalda, D. Sitkoff and B. Honig, *J. Phys. Chem.*, 1996, **100**, 11775–11788.
26 D. A. Edwards, S. D. Edwards, W. R. Martin, T. J. Pringle and P. Thornton, *Polyhedron*, 1992, **11**, 1569–1573.
27 J. Granifo, S. J. Bird, K. G. Orrell, A. G. Osborne and V. Sik, *Inorg. Chim. Acta*, 1999, **295**, 56–63.
28 Despite repeated attempts to obtain better elemental analysis data, the low oxidation potential of this compound resulted in lower than expected C and N values.